JCI The Journal of Clinical Investigation

$G_s\alpha$ deficiency in the dorsomedial hypothalamus underlies obesity associated with $G_s\alpha$ mutations

Min Chen, … , Oksana Gavrilova, Lee S. Weinstein

J Clin Invest. 2016. https://doi.org/10.1172/JCI88622.

Research Article **Metabolism**

$G_s\alpha$, encoded by *Gnas*, mediates hormone and neurotransmitter receptor–stimulated cAMP generation. Heterozygous $G_s\alpha$-inactivating mutations lead to obesity in Albright hereditary osteodystrophy (AHO) patients, but only when the mutations occur on the maternal allele. This parent-of-origin effect is due to $G_s\alpha$ imprinting in the CNS, although the relevant CNS regions are unknown. We have now shown that mice with a *Gnas* gene deletion disrupting $G_s\alpha$ expression on the maternal allele, but not the paternal allele, in the dorsomedial nucleus of the hypothalamus (DMH) developed obesity and reduced energy expenditure without hyperphagia. Although maternal *Gnas* deletion impaired activation of brown adipose tissue (BAT) in mice, their responses to cold environment remained intact. Similar findings were observed in mice with DMH-specific deficiency of melanocortin MC4R receptors, which are known to activate $G_s\alpha$. Our results show that $G_s\alpha$ imprinting in the DMH underlies the parent-of-origin metabolic phenotype that results from $G_s\alpha$ mutations and that DMH MC4R/$G_s\alpha$ signaling is important for regulation of energy expenditure and BAT activation, but not the metabolic response to cold.

$G_s\alpha$ deficiency in the dorsomedial hypothalamus underlies obesity associated with $G_s\alpha$ mutations

Min Chen,[1] Yogendra B. Shrestha,[1] Brandon Podyma,[1] Zhenzhong Cui,[2] Benedetta Naglieri,[1] Hui Sun,[1] Thuy Ho,[1] Eric A. Wilson,[1] Yong-Qi Li,[1] Oksana Gavrilova,[2] and Lee S. Weinstein[1]

[1]Metabolic Diseases Branch and [2]Mouse Metabolism Core Laboratory, National Institute of Diabetes, Digestive, and Kidney Diseases, NIH, Bethesda, Maryland, USA.

$G_s\alpha$, encoded by *Gnas*, mediates hormone and neurotransmitter receptor–stimulated cAMP generation. Heterozygous $G_s\alpha$-inactivating mutations lead to obesity in Albright hereditary osteodystrophy (AHO) patients, but only when the mutations occur on the maternal allele. This parent-of-origin effect is due to $G_s\alpha$ imprinting in the CNS, although the relevant CNS regions are unknown. We have now shown that mice with a *Gnas* gene deletion disrupting $G_s\alpha$ expression on the maternal allele, but not the paternal allele, in the dorsomedial nucleus of the hypothalamus (DMH) developed obesity and reduced energy expenditure without hyperphagia. Although maternal *Gnas* deletion impaired activation of brown adipose tissue (BAT) in mice, their responses to cold environment remained intact. Similar findings were observed in mice with DMH-specific deficiency of melanocortin MC4R receptors, which are known to activate $G_s\alpha$. Our results show that $G_s\alpha$ imprinting in the DMH underlies the parent-of-origin metabolic phenotype that results from $G_s\alpha$ mutations and that DMH MC4R/$G_s\alpha$ signaling is important for regulation of energy expenditure and BAT activation, but not the metabolic response to cold.

Introduction

Albright hereditary osteodystrophy (AHO) is a monogenic obesity disorder caused by heterozygous loss-of-function mutations of $G_s\alpha$ (encoded by *Gnas*), a ubiquitously expressed G protein that couples hormone and neurotransmitter receptors to intracellular cAMP generation. AHO patients develop obesity (1), reduced energy expenditure (2), and insulin resistance (3), but only when the mutation is present on the maternal allele. Similar parent-of-origin–specific metabolic effects are present in mice with heterozygous germline deletion of *Gnas* exon 1 on the maternal ($E1^{m-}$) and paternal ($E1^{p-}$) alleles (4–6). These parent-of-origin effects are due to *Gnas* imprinting, which leads to $G_s\alpha$ being primarily expressed from the maternal allele in certain tissues (7). In these tissues, a loss-of-function $G_s\alpha$ mutation on the active maternal allele leads to severe $G_s\alpha$ deficiency and can lead to a phenotype, whereas the same mutation on the inactive paternal allele has little effect on $G_s\alpha$ expression and therefore produces little or no phenotype.

Studies in mice with maternal (mBrGsKO) and paternal (pBrGsKO) heterozygous $G_s\alpha$ mutations limited to the CNS demonstrate that the parent-of-origin–specific metabolic phenotype results from $G_s\alpha$ imprinting within one or more CNS regions, as the same metabolic phenotype was observed in mBrGsKO but not pBrGsKO mice (8). The obesity associated with maternal $G_s\alpha$ mutations is due to reduced sympathetic nervous system (SNS) activity and energy expenditure and not to hyperphagia (2, 4, 5, 8). Several hypothalamic nuclei, including the paraventricular nucleus (PVN), ventromedial nucleus (VMH), and dorsomedial nucleus (DMH), are involved in regulation of energy and glucose metabolism. However, G_s mutations within the PVN (9) or VMH (10) do not produce the metabolic phenotype seen in $E1^{m-}$ or mBrGsKO mice. Therefore, the CNS site or sites where $G_s\alpha$ is imprinted that accounts for the metabolic phenotype seen in AHO patients and mice with maternal $G_s\alpha$ mutations remain unknown.

Central melanocortins are neurotransmitters that promote negative energy balance by stimulating energy expenditure and inhibiting food intake, primarily via MC4R receptors, which are known to activate $G_s\alpha$ (11). mBrGsKO mice have impaired stimulation of energy expenditure in response to the melanocortin agonist melanotan II (MTII), while the ability of MTII to inhibit food intake in these mice is unaffected (8). It therefore appears that melanocortins stimulate energy expenditure by signaling through $G_s\alpha$ at a CNS site other than the PVN (9, 12). In this study, we show that $G_s\alpha$ is imprinted in the DMH, that the metabolic phenotype associated with maternal $G_s\alpha$ mutations is due to $G_s\alpha$ deficiency in the DMH, and that loss of MC4R in the DMH leads to a similar metabolic phenotype. Moreover, DMH-specific loss of MC4R and $G_s\alpha$ signaling leads to reduced brown adipose tissue (BAT) activation, but does not affect the ability of a cold environment to activate BAT.

Results

$G_s\alpha$ is imprinted in DMH. We examined $G_s\alpha$ gene expression in the DMH of mice with either maternal (referred to hereafter as $E1^{m-}$) or paternal (referred to hereafter as $E1^{p-}$) heterozygous germline *Gnas* deletions by in situ hybridization. DMH $G_s\alpha$ mRNA levels in $E1^{p-}$ mice were approximately 70% of those in controls, while DMH $G_s\alpha$ mRNA levels in $E1^{m-}$ mice were only approximately 30% of those in controls (Figure 1, A and B), indicating that $G_s\alpha$ is imprinted in the DMH with preferential expression from the maternal allele. The residual DMH $G_s\alpha$ expression observed in $E1^{m-}$ mice may indicate that imprinting in DMH neurons is not complete or that $G_s\alpha$ is

Authorship note: M. Chen and Y.B. Shrestha are co–first authors.
Conflict of interest: The authors have declared that no conflict of interest exists.
Submitted: May 17, 2016; **Accepted:** November 10, 2016.
Reference information: *J Clin Invest*. doi:10.1172/JCI88622.

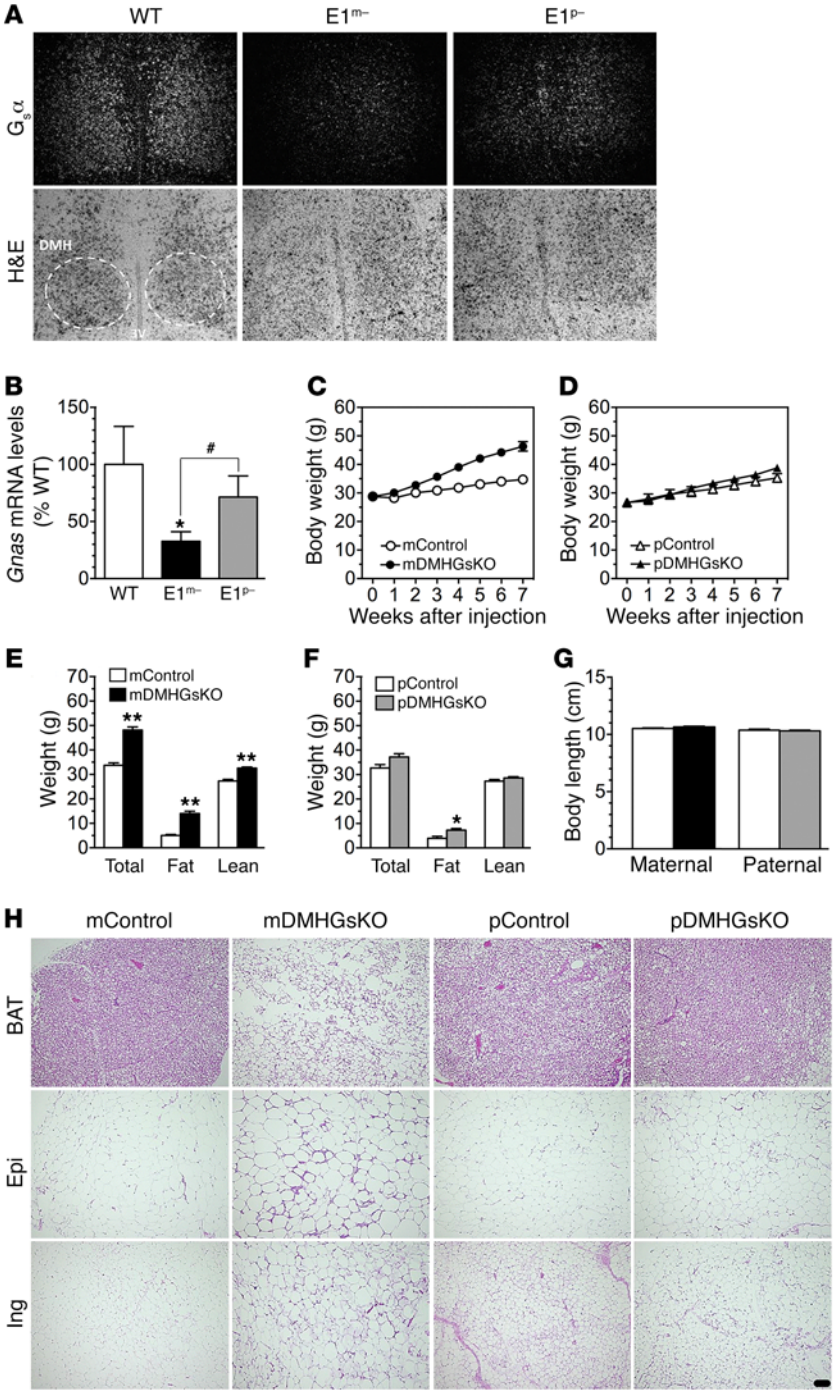

Figure 1. Gsα is imprinted in the DMH. (**A** and **B**) $G_s\alpha$ mRNA levels in the DMH (indicated with dashed outline) of WT mice and mice with germline heterozygous *Gnas* deletion on either the maternal ($E1^{m-}$) or paternal ($E1^{p-}$) allele (upper panel: dark field showing $G_s\alpha$ expression; lower panel: H&E staining). Original magnification: ×20. (**B**) Quantification of in situ hybridization study with $G_s\alpha$ mRNA levels expressed as percentage of WT. n = 5–8/group. $^*P < 0.05$, $E1^{m-}$ vs. WT; $^{\#}P < 0.05$, $E1^{m-}$ vs. $E1^{p-}$. (**C** and **D**) Body weight curves of (**C**) male mDMHGsKO and (**D**) pDMHGsKO mice and their control littermates. (**E** and **F**) Body composition of (**E**) mDMHGsKO and (**F**) pDMHGsKO mice and their control littermates at 2 to 2.5 months after AAV injection (n = 5–10/group). ($^*P < 0.05$ or $^{**}P < 0.01$ vs. controls by Student's t test.) (**G**) Body length of mDMHGsKO (left) and pDMHGsKO (right) mice and their respective controls at 4 to 5 months after injection (n = 5–14/group). (**H**) Histology of BAT, epididymal WAT (Epi), and inguinal WAT (Ing) from mDMHGsKO and pDMHGsKO mice and their respective controls (H&E staining). Scale bar: 100 μm. Data are shown as mean ± SEM.

not imprinted in other cell types (e.g., vascular, stroma) within the region that would be included in the samples analyzed.

Maternal, but not paternal, $G_s\alpha$ deletion in DMH leads to obesity. Mice with DMH-specific deletion within the maternal (mDMHGsKO mice) or paternal (pDMHGsKO mice) $G_s\alpha$ allele were generated by bilateral stereotaxic injection of AAV-Cre-GFP into the DMH of male maternal (referred to hereafter as $E1^{fl/+}$) or paternal (referred to hereafter as $E1^{+/fl}$) *Gnas*-floxed mice at 6 to 7 weeks of age (Supplemental Figure 1A; supplemental material available online with this article; https://doi.org/10.1172/JCI88622DS1). $G_s\alpha$-floxed littermates simultaneously injected with AAV-GFP (lacking Cre) were used as controls. mDMHGsKO mice gradually gained more weight than control mice (Figure 1C) and were 38% heavier at 4 to 5 months after injection (mDMHGsKO 51 ± 1 g vs. control 37 ± 1 g), while pDMHGsKO mice gained weight at a rate similar to that of controls (Figure 1D). Increased weight gain was only observed in mDMHGsKO mice in which AAV-Cre-GFP was correctly targeted to the DMH bilaterally, while mice in which only one side was correctly targeted showed normal body weight (Supplemental Figure 1, B and C). Only mice in which viral injection was correctly targeted bilaterally are included in the further analysis.

Consistent with increased body weight, mDMHGsKO mice had marked increased fat mass (Figure 1E) with greater lipid accumulation within adipocytes in interscapular BAT and epididymal and inguinal white adipose tissue (WAT) (Figure 1H). mDMHGsKO mice also had a small but significant increase in lean body mass (Figure 1E). The increased thickening between lipid droplets in WAT of mDMHGsKO mice is at least partially explained by increased inflammation and macrophage invasion, as these sections showed increased immunohistochemical staining for the macrophage-specific marker F4/80 (Supplemental Figure 2). In contrast to mDMHGsKO mice, pDMHGsKO mice showed only a small increase in fat mass (Figure 1F) and no obvious changes in BAT or WAT histology (Figure 1H). In line with their increased adiposity, mDMHGsKO mice had a 5-fold increase in serum leptin levels (at 4 to 5 months after injection), while leptin levels were only 2-fold higher in pDMHGsKO mice (Table 1). Body length was not affected in either mDMHGsKO or pDMHGsKO mice (Figure 1G). This parent-of-origin effect of DMH $G_s\alpha$ muta-

Table 1. Serum chemistries in mDMHGsKO, pDMHGsKO, and control mice

	mControl	mDMHGsKO	pControl	pDMHGsKO
Glucose, fasted (mg/dl)	78 ± 7	122 ± 29[A]	78 ± 9	90 ± 7
Insulin, fasted (ng/ml)	0.3 ± 0.2	0.4 ± 0.2	0.3 ± 0.1	0.6 ± 0.1
Insulin, fed (ng/ml)	2.1 ± 0.7	70.5 ± 19.7[B]	2.1 ± 0.5	6.8 ± 2.5
Free fatty acids (mM)	0.41 ± 0.05	0.40 ± 0.06	0.39 ± 0.04	0.44 ± 0.08
Triglycerides (mg/dl)	147 ± 31	236 ± 33	203 ± 28	223 ± 22
Cholesterol (mg/dl)	173 ± 19	214 ± 17	173 ± 8	182 ± 7
Leptin (ng/ml)	9.5 ± 2.2	48.2 ± 6.1[B]	8.6 ± 1.3	17.7 ± 3.4[B]
T3 (ng/ml)	0.79 ± 0.15	0.78 ± 0.12	0.48 ± 0.10	0.51 ± 0.08
T4 (μg/dl)	3.48 ± 0.35	2.92 ± 0.26	3.27 ± 0.24	3.54 ± 0.17
Corticosterone (ng/ml)	200 ± 44	186 ± 28	232 ± 72	203 ± 73

All results are in fed mice except where noted otherwise. Data are shown as mean ± SEM. [A]P <0.01; [B]P < 0.05 vs. controls by Student's t test; n = 5–8/group.

tion on obesity is consistent with $G_s\alpha$ being imprinted in the DMH. There were no differences in serum triiodothyronine (T3), L-thyroxine (T4), or corticosterone levels between groups of mice (Table 1).

Obesity in mDMHGsKO mice is associated with reduced energy expenditure. We observed no differences in daily food intake (normalized by body weight) between mDMHGsKO and control mice at 2 months after injection (Figure 2A) or at 2 weeks after injection (in kcal/d) before the development of obesity in mDMHGsKO mice (Figure 2C). Therefore, obesity in mDMHGsKO mice is not primarily a result of hyperphagia. Food intake was also unaffected in pDMHGsKO mice (Figure 2B).

Both resting energy expenditure (REE) and total energy expenditure (TEE) were significantly reduced in mDMHGsKO mice at ambient temperature (22°C), but were unaffected at thermoneutral temperature (30°C), a temperature at which SNS stimulation of thermogenesis is minimized (Figure 2F), a finding consistent with impaired SNS activation in response to an environmental temperature below thermoneutrality. mDMHGsKO mice also had low total and ambulatory activity levels at 22°C and low total activity levels at 30°C (Figure 2H). In contrast to mDMHGsKO mice, pDMHGsKO mice had normal energy expenditure and activity levels except for reduced ambulatory activity at 22°C (Figure 2, G and I). Respiratory exchange ratios (vCO_2/vO_2) were unaffected in both mDMHGsKO and pDMHGsKO mice (data not shown). Overall obesity in mDMHGsKO mice was associated with reduced energy expenditure with little effect on food intake.

Impaired melanocortin stimulation of energy expenditure in mDMHGsKO mice. We examined the acute energy expenditure and food intake responses to the MC3R/MC4R agonist MTII in mDMHGsKO and pDMHGsKO mice. mDMHGsKO mice showed impaired stimulation of energy expenditure in response to MTII (Figure 2J). In contrast, the ability of MTII to inhibit food intake was similar in mDMHGsKO and control mice (Figure 2D; both groups of mice showed an approximately 60% reduction in food intake after MTII when compared with a saline injection). Both energy expenditure and food intake responses to MTII were unaffected in pDMHGsKO mice (Figures 2, E and K). The responses to MTII in mDMHGsKO mice are consistent with these mice having reduced energy expenditure and normal food intake.

Maternal, but not paternal, Gnas deletion in DMH leads to glucose intolerance and insulin resistance. At 2 to 2.5 months after injection, mDMHGsKO mice had elevated fasting blood glucose levels (Table 1). Serum insulin levels were unaffected while fasting, but were strikingly elevated in the fed state (Table 1). At this time point, mDMHGsKO mice also had impaired glucose tolerance (Figure 3A) and insulin sensitivity (Figure 3C). In contrast, all of these parameters were unaffected in pDMHGsKO mice (Figure 3, B and D; Table 1). Serum-free fatty acid, triglyceride, and cholesterol levels were not significantly different between groups, although triglycerides and cholesterol tended to be higher in mDMHGsKO mice (Table 1).

In contrast to what was observed in obese mDMHGsKO mice at 2 to 2.5 months after injection, mDMHGsKO mice showed no differences in fasting glucose (Figure 3G) or insulin levels (Figure 3H, time point 0) or in glucose tolerance (Figure 3E) at 2 weeks after injection before the development of obesity (Figure 3F). Insulin levels were elevated at time point 120 minutes of the glucose tolerance test (Figure 3H). These results suggest that $G_s\alpha$ deficiency in the DMH does not primarily affect glucose metabolism independently of obesity.

Cold-induced thermogenesis is intact in both mDMHGsKO and pDMHGsKO mice. The DMH is a key hypothalamic region governing SNS stimulation of BAT thermogenesis (13, 14). Consistent with histology showing inactive BAT in mDMHGsKO mice (Figure 1H), expression of several BAT genes involved in thermogenesis, including those for PPARγ coactivator 1-α (*Pgc1a*), cytochrome *c* (Figure 4A), and uncoupling protein 1 (*Ucp1*) (Figure 4D , RT) were significantly reduced in mDMHGsKO mice. Despite these differences in BAT activation, mDMHGsKO mice had normal baseline body temperature (mDMHGsKO 36.7 ± 0.2°C vs. maternal control [mControl] 36.8 ± 0.3°C) and were able to maintain normal body temperature while placed at 4°C for 6 hours (Figure 4C). While BAT *Ucp1* gene expression in mDMHGsKO mice was decreased at room temperature, its induction in response to cold was fully intact in these mice (Figure 4D), consistent with their ability to maintain normal body temperature in the cold. All of these parameters were unaffected in pDMHGsKO mice (Figure 4, B, C, and E).

We also examined the response of both interscapular BAT and inguinal WAT to chronic cold adaptation. Mice were placed in chambers in which environmental temperature was reduced by 2°C per day over 8 days and then kept at 6°C for 7 days. Similarly to what occurred in the acute cold experiments, a normal body temperature was maintained throughout the experiment and BAT *Ucp1* mRNA was induced normally in both mDMHGsKO and pDMHGsKO mice (Supplemental Figure 3, A–C). BAT histology confirmed that both groups of mutants showed smaller BAT adipocytes with reduced lipid content, a pattern consistent with increased BAT activation (Supplemental Figure 3D). In addition, both sets of mutants showed areas of increased "browning" of inguinal WAT, as determined by increased UCP1 protein expression by immunohistochemistry (Supplemental Figure 3E). These

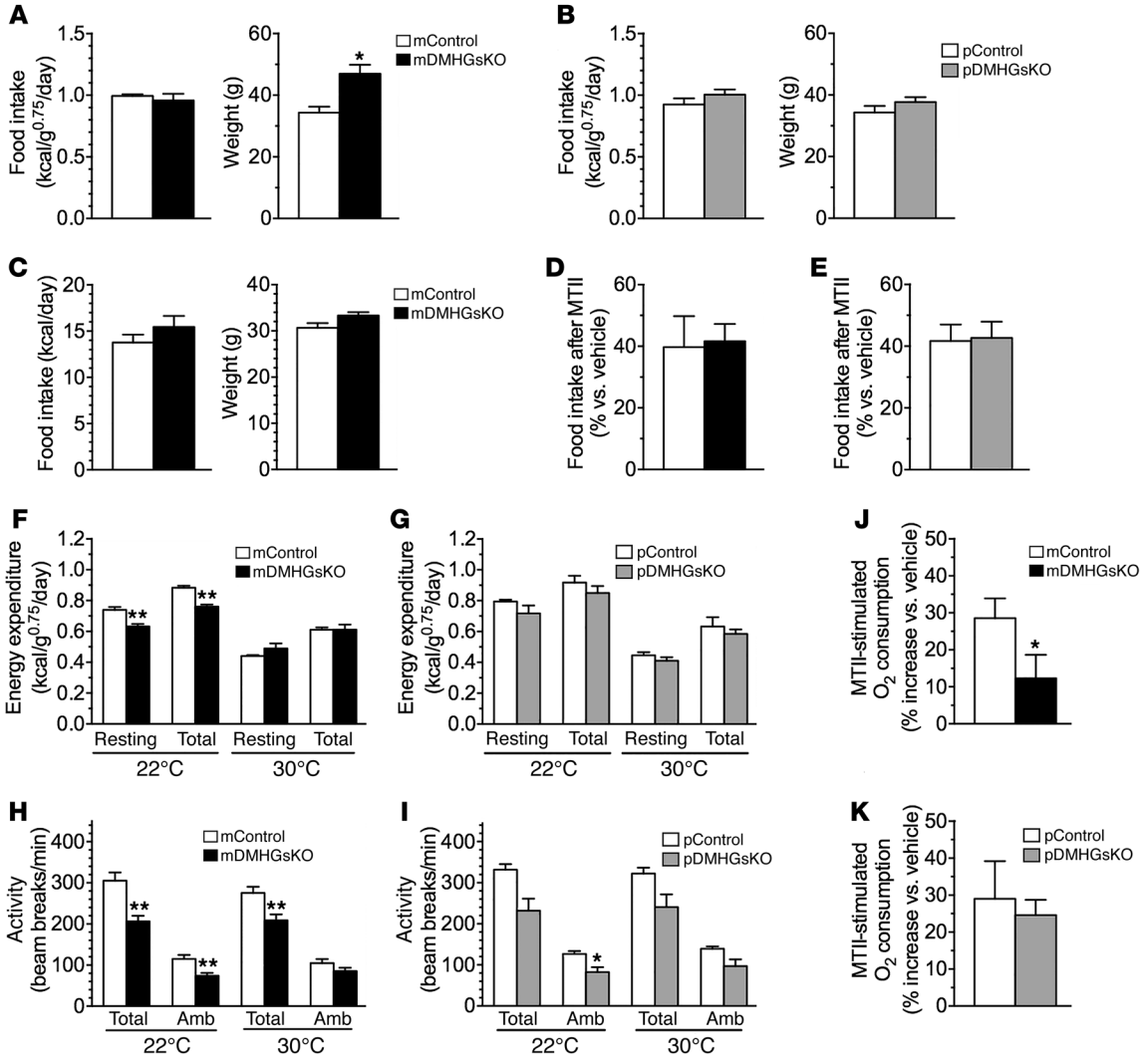

Figure 2. Reduced energy expenditure in mDMHGsKO, but not pDMHGsKO mice. (**A**) Food intake (left) and body weight (right) of mDMHGsKO and control mice (n = 4–5/group). (**B**) Food intake (left) and body weight (right) of pDMHGsKO and control mice (n = 4/group). Food intake was measured at 2 months after viral injection and is normalized to body weight. (**C**) Absolute food intake (kcal/d, left) and body weight (right) of young mDMHGsKO and control mice at 2 weeks after injection (n = 7–10/group). (**D** and **E**) Food intake response to MC4R agonist MTII (expressed as percentage of intake vs. intake after vehicle injection) in (**D**) mDMHGsKO mice (n = 7–10/group) and (**E**) pDMHGsKO mice (n = 4/group) and their respective controls. (**F** and **G**) REE and TEE at 22°C and 30°C in (**F**) mDMHGsKO mice and (**G**) pDMHGsKO mice and their respective controls at 2 to 2.5 months after viral injection (n = 7–12/group). (**H** and **I**) Total and ambulatory (Amb) activity levels in (**H**) mDMHGsKO mice and (**I**) pDMHGsKO mice and their respective controls (n = 7–12/group). (**J** and **K**) Increase in energy expenditure in response to MTII in (**J**) mDMHGsKO mice (n = 6–10/group) and (**K**) pDMHGsKO (n = 6) and their respective controls. Data are shown as mean ± SEM. *P < 0.05; **P < 0.01 vs. controls by Student's t test.

results confirm that both BAT activation and WAT "browning" in response to cold are preserved in mDMHGsKO mice.

The DMH has been shown to also regulate cardiac SNS activity via sympathetic premotor neurons in the rostral medullary raphe region and to mediate stress-induced tachycardia (15–18). mDMHGsKO mice had significantly reduced heart rate (Figure 4F) with normal blood pressure (Figure 4G), suggesting that $G_s\alpha$ signaling in the DMH is important in regulating cardiac SNS activity. Neither heart rate nor blood pressure was affected in pDMHGsKO mice (Figure 4, F and G).

MC4R deficiency in DMH leads to a phenotype similar to that of mDMHGsKO mice. To determine whether the mDMHGsKO metabolic phenotype may be due to loss of MC4R-$G_s\alpha$ signaling in the DMH, we generated mice with homozygous DMH-specific *Mc4r* deletion (DMH-MC4RKO) by bilateral injection of AAV-Cre-GFP into the DMH of homozygous *Mc4r*-floxed mice, while mice injected with AAV-GFP served as controls. Loss of MC4R expression in the DMH was confirmed by in situ hybridization (Figure 5A). Overall, DMH-MC4RKO mice had a phenotype very similar to that of mDMHGsKO mice, including a large increase in body weight and fat mass with a smaller increase in lean mass (Figure 5, B and C), a large increase in serum leptin levels (Supplemental Table 1), and increased lipid accumulation in BAT and WAT adipocytes (Figure 5L). DMH-MC4RKO mice had a very small but significant increase in body length (Figure 5D). Similarly to mDMHGsKO mice, DMH-MC4RKO mice had unchanged food intake (Figure 5, G and H), but significantly reduced energy expenditure (Figure 5E), while activity levels were unaffected (Figure 5F). MTII stimulation of energy

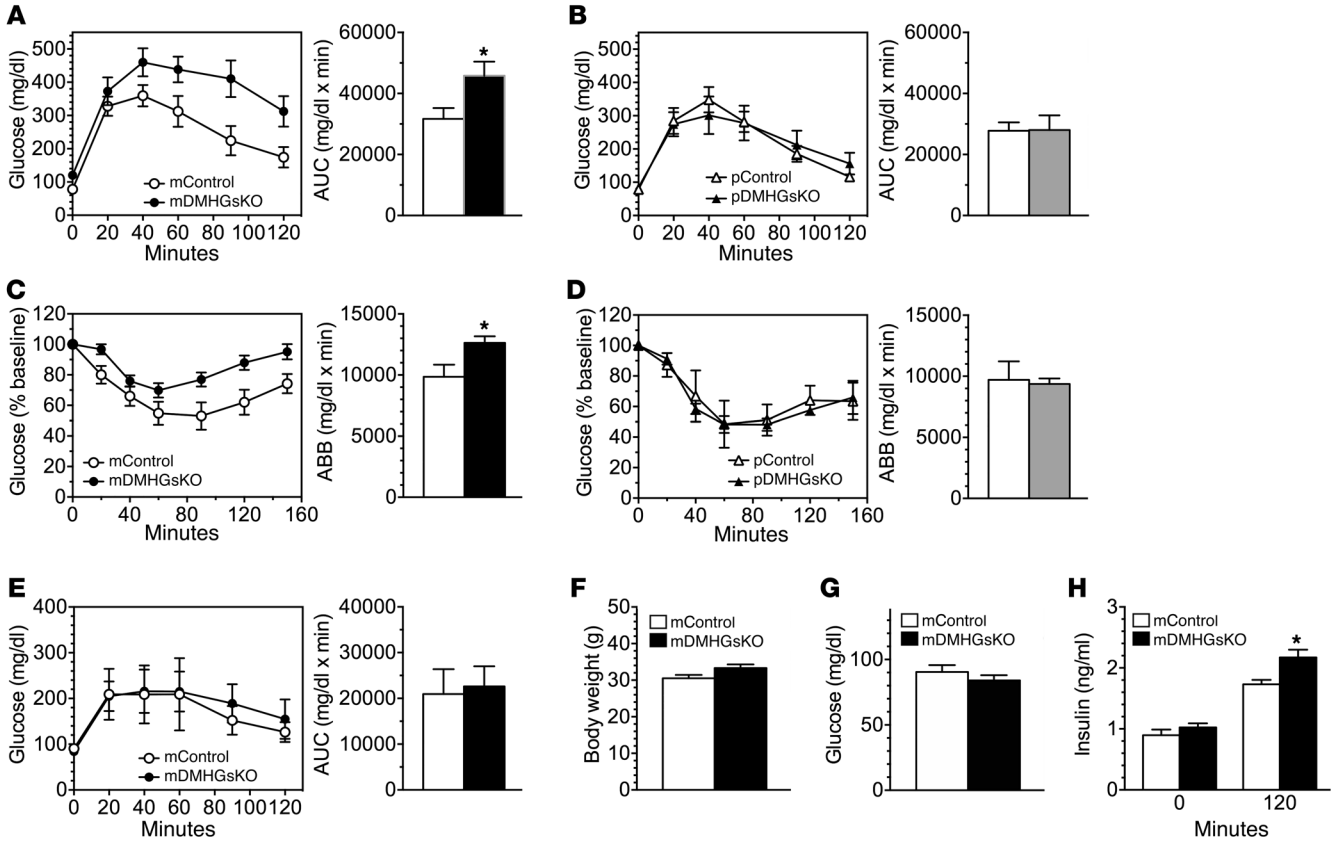

Figure 3. Glucose metabolism in mDMHGsKO and pDMHGsKO mice. (**A** and **B**) Results of glucose tolerance tests (glucose curve, left; AUC, right) performed on (**A**) mDMHGsKO mice (n = 7–9/group) and (**B**) pDMHGsKO mice (n = 5–7/group) and their respective controls. (**C** and **D**) Results of insulin tolerance tests (glucose curves as percentage of baseline, left; area below baseline [ABB], right) performed in (**C**) mDMHGsKO mice (n = 7–10/group) and (**D**) pDMHGsKO mice (n = 4–6/group) and their respective controls. Experiments in parts **A**–**D** were performed in mice at 2.5 to 3 months after injection. (**E**) Glucose tolerance test (glucose curve, left; AUC, right) performed on mDMHGsKO and control mice at 2 weeks after injection (n = 4–6/group). (**F**) Body weight of mice at the time of glucose tolerance tests shown in part **E**. (**G**) Fasting blood glucose levels in mDMHGsKO and control mice at 2 weeks after viral injection. (**H**) Serum insulin levels at time 0 and 120 minutes during glucose tolerance tests shown in part **E**. Data are shown as mean ± SEM. *P < 0.05 vs. controls by Student's t test.

expenditure was impaired (Figure 5I), while the MTII effect on food intake was unaffected (Figure 5J). DMH-MC4RKO mice were also able to maintain body temperature at 4°C (Figure 5K) despite having relatively inactive BAT based upon histology (Figure 5L). During the same experiments, the ability of cold to increase UCP1 protein expression was not impaired in DMH-MC4RKO mice (Supplemental Figure 4), suggesting that MC4R signaling in DMH is not required for BAT activation in response to cold.

DMH-MC4RKO mice studied at 2 to 2.5 months after injection (at a time when they were obese) also had elevated fasting insulin levels (Supplemental Table 1) and impaired glucose tolerance (Supplemental Figure 5A) and insulin sensitivity (Supplemental Figure 5B). Serum-free fatty acids and triglycerides were unaffected, while serum cholesterol was elevated in DMH-MC4RKO mice (Supplemental Table 1). However, similarly to what we observed in mDMHGsKO mice, DMH-MC4RKO mice examined at 2 weeks after injection when the mice had similar body weight (Supplemental Figure 5E) showed no significant change in glucose tolerance (Supplemental Figure 5C), fasting glucose (72 ± 5 vs. 70 ± 5 mg/dl, n = 5–7), or fasting insulin (Supplemental Figure 5D). Overall, our results suggest that the metabolic changes observed in mDMHGsKO mice can be mostly, if not completely, accounted for by loss of MC4R signaling in the DMH.

To confirm that loss of $G_s\alpha$ in the DMH also leads to loss of MC4R signaling in this region, we examined the phosphorylation of cAMP-response element–binding protein (CREB), a downstream response to $G_s\alpha$-cAMP–protein kinase A activation, in mDMHGsKO and control mice at 1 hour after i.p. MTII administration. We examined the dorsal and compact areas of the DMH, as these have been shown to be the regions where MC4R is expressed (19, 20). The extent of phosphorylated CREB (pCREB) staining was significantly reduced in the DMH of mDMHGsKO mice as compared with controls, while the extent of staining for total CREB protein was similar between the 2 groups (Figure 6).

Absence of metabolic effect in mice with loss of $G_s\alpha$ expression in other CNS regions. We previously showed that $G_s\alpha$ mutations in SIM1 neurons (present in PVN and other sites) (9) and SF1 neurons (present in VMH) (10) do not replicate the metabolic phenotype seen in maternal germline $G_s\alpha$–deficient ($E1^{m-}$) (4) and maternal whole-brain $G_s\alpha$–deficient (mBrGsKO) (8) mice. Here, we further show that heterozygous $G_s\alpha$ deletions in serotonergic neurons (including raphe), agouti-related peptide-expressing

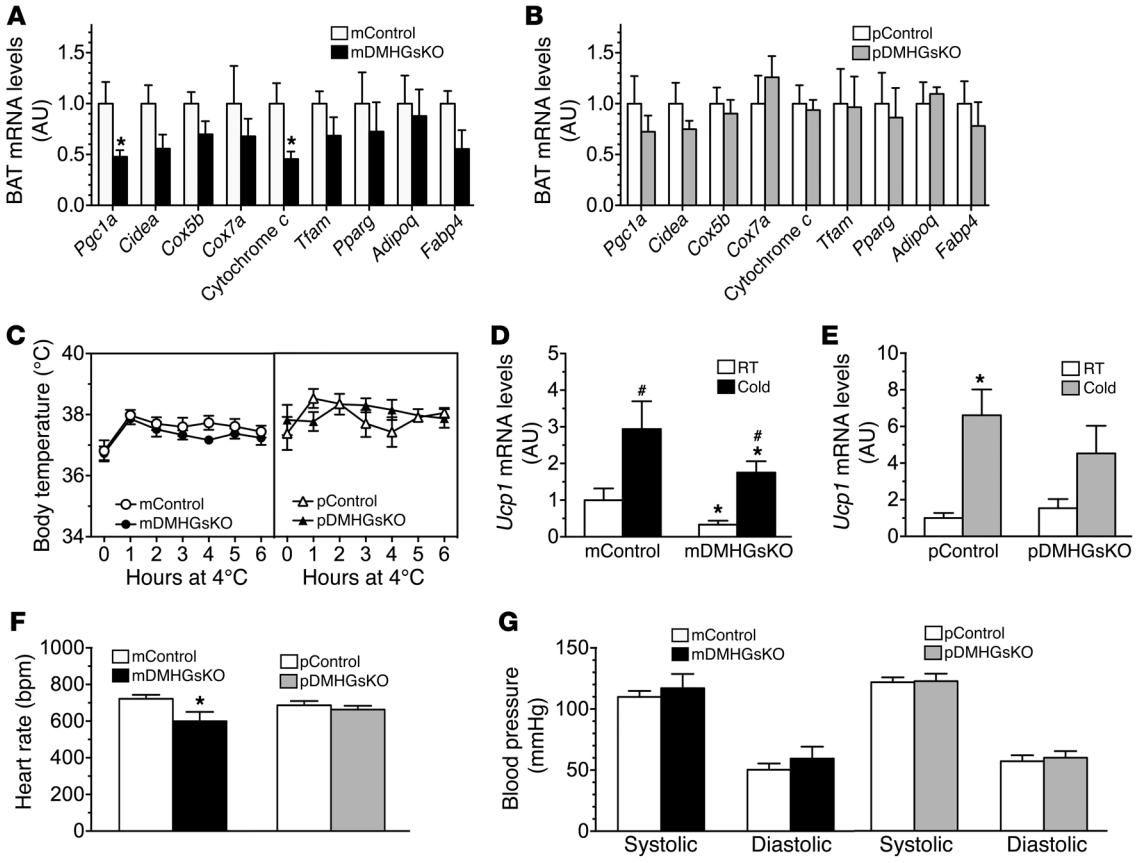

Figure 4. Cold tolerance and cardiovascular function in mDMHGsKO and pDMHGsKO mice. (**A** and **B**) Relative BAT gene expression in (**A**) mDMHGsKO mice and (**B**) pDMHGsKO mice and their respective controls (n = 5–6/group). (**C**) Rectal temperature before (0 hours) and after exposure to 4°C for 6 hours (left panel, mDMHGsKO and control mice [n = 9–13/group]; right panel, pDMHGsKO and control mice [n = 4–6/group]). (**D** and **E**) BAT *Ucp1* gene expression at room temperature (RT) and after 6 hours at 4°C (cold) in (**D**) mDMHGsKO mice and (**E**) pDMHGsKO mice and their respective controls (n = 5–10/group). $^{\#}P < 0.05$ vs. room temperature; $^{*}P < 0.05$ vs. controls. (**F**) Heart rate and (**G**) blood pressure in mDMHGsKO mice and pDMHGsKO mice and their respective controls (n = 6–7/group). Data are shown as mean ± SEM. $^{*}P < 0.05$ vs. controls by Student's t test (with correction for repeated measures for parts **A** and **B**).

(Agrp-expressing) neurons, and cholinergic neurons generated by mating maternal and paternal $G_s\alpha$-floxed mice with tryptophan hydroxylase 2–*Cre*, (*Tph2-Cre*), *Agrp-Cre*, and choline acetyltransferase–*Cre* (*Chat-Cre*) mouse lines, respectively, had no effects on body weight or glucose metabolism (Figure 7).

Discussion

In this study, we show that $G_s\alpha$ is imprinted in the DMH and that the effects of maternal $G_s\alpha$ mutations in mice (and likely AHO patients) on adiposity, energy expenditure, BAT activation, and heart rate result from $G_s\alpha$ deficiency in the DMH due to the combined effects of mutation on the maternal allele and silencing of the paternal allele secondary to imprinting. In contrast, results from this and prior studies (9, 10) show that the same parent-of-origin–specific metabolic phenotype could not be replicated by deleting the maternal *Gnas* allele in the PVN, VMH, AgRP neurons, serotonergic neurons, and cholinergic neurons.

MC4R mutations are the most common cause of severe early onset obesity and are associated with hyperphagia, reduced energy expenditure, increased body length, impaired BAT thermogenesis, insulin resistance, and reduced heart rate and blood pressure (21–23). Prior studies suggest that MC4R actions on food intake and body length occur primarily in the PVN and involve the relatively PVN-specific transcription factor Sim1 (12, 24–26). These manifestations of impaired MC4R signaling are not replicated in mice with either whole brain– or PVN-specific $G_s\alpha$ mutation (8, 9). We recently showed that the effects of MC4R action in the PVN on food intake and body length are mediated via $G_{q/11}\alpha$ rather than $G_s\alpha$ (27).

The effect of DMH-specific $G_s\alpha$ deficiency on energy expenditure and thermogenesis may reflect loss of MC4R action in the DMH, as MC4R is expressed in this region (19, 20) and MC4R activation leads to stimulation of energy expenditure and BAT activation (28–30). We confirmed that loss of either MC4R or $G_s\alpha$ in the DMH leads to obesity associated with reduced energy expenditure and impaired stimulation of energy expenditure in response to an MC4R agonist, showing that MC4R-$G_s\alpha$ signaling is an important pathway in mediating the effects of melanocortins on energy expenditure. Our present model of the sites of action and G proteins involved in MC4R regulation of food intake, thermogenesis, and energy expenditure is summarized in Supplemental Figure 6.

The DMH contains neurons that are polysynaptically connected to BAT via the rostral raphe pallidus and that stimulate SNS activity to BAT, resulting in induction of *Ucp1*, increased lipid oxi-

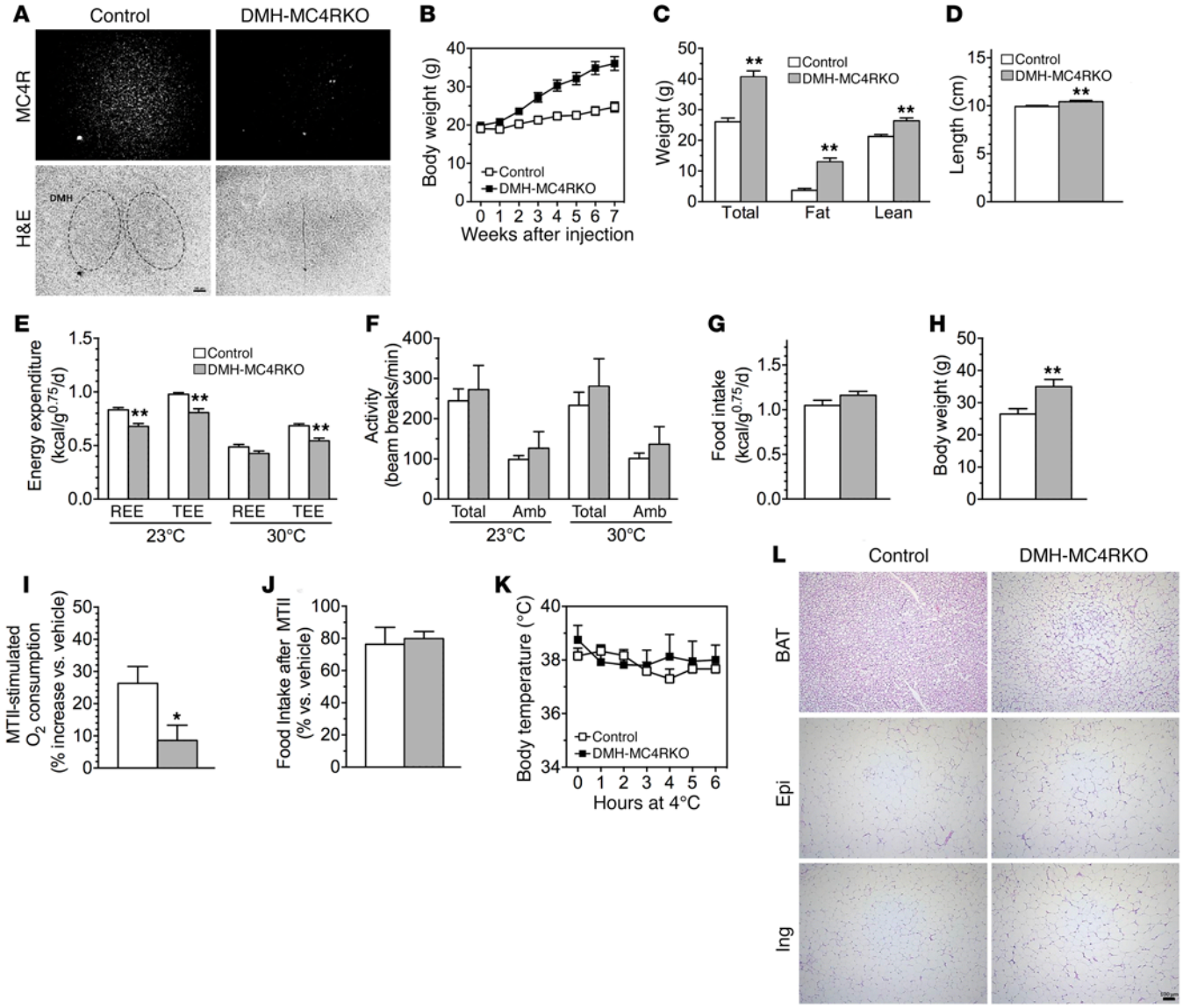

Figure 5. DMH-MC4RKO mice develop obesity with reduced energy expenditure. (**A**) *Mc4r* gene expression in DMH of control (AAV-GFP injected MC4R floxed) and DMH-MC4RKO (AAV-Cre injected *Mc4r* floxed) mice assessed by in situ hybridization (upper panels, dark field showing *Mc4r* expression; lower panels, H&E staining with DMH outlined). (**B**) Body weight curves (n = 12–14/group), (**C**) body composition (n = 7–8/group), and (**D**) body length (n = 10/group) in DMH-MC4RKO and control mice. (**E** and **F**) (**E**) REE and TEE and (**F**) total and ambulatory activity levels in DMH-MC4RKO and control mice at 22°C and 30°C (n = 7–8/group). (**G** and **H**) (**G**) Food intake and (**H**) body weight at the time of food intake measurement (n = 9/group). (**I** and **J**) (**I**) Acute energy expenditure (n = 5–6/group) and (**J**) food intake (n = 4/group) responses to MTII as compared with vehicle. (**K**) Cold tolerance test (n = 4–6/group). (**L**) Histology of BAT, epididymal WAT, and inguinal WAT from DMH-MC4RKO and control mice (H&E staining). Scale bar: 100 μm. All experiments were performed 2 to 2.5 months after viral injection. Data are shown as mean ± SEM. *P < 0.05; **P < 0.01 vs. controls by Student's t test.

dation, and thermogenesis (14, 31–34). We observed that mDMHGsKO mice had an inactive BAT appearance and reduced expression of thermogenic genes in BAT (e.g., *Pgc1a*, cytochrome *c*, and *Ucp1*), and similar BAT histology was observed in DMH-MC4RKO mice. These findings implicate DMH MC4R-$G_s\alpha$ signaling in SNS activation of BAT and are consistent with a prior study showing that MTII stimulation of BAT requires MC4R activation in DMH (35).

Despite having relatively inactive BAT at room temperature, both mDMHGsKO and DMH-MC4RKO mice were able to maintain a normal body temperature when kept at 4°C for up to 6 hours, and both groups of mice were able to normally increase BAT UCP1 expression in response to cold, indicating that DMH MC4R-$G_s\alpha$ signaling is not required for cold-induced BAT thermogenesis. In addition, we showed that WAT "browning" in response to cold is also intact in mDMHGsKO mice. The ability of mDMHGsKO mice to maintain normal cold responsiveness likely reflects the fact that inputs to the DMH in the cold-reflex neural circuit are primarily GABAnergic neurons from the medial preoptic area that do not transmit their signal via $G_s\alpha$ (36, 37). $G_s\alpha$ pathways within other CNS regions are likely to be involved in cold-induced BAT activation, as responsiveness to cold is impaired in mBrGsKO mice (9). However, we cannot completely rule out a role for $G_s\alpha$ in DMH

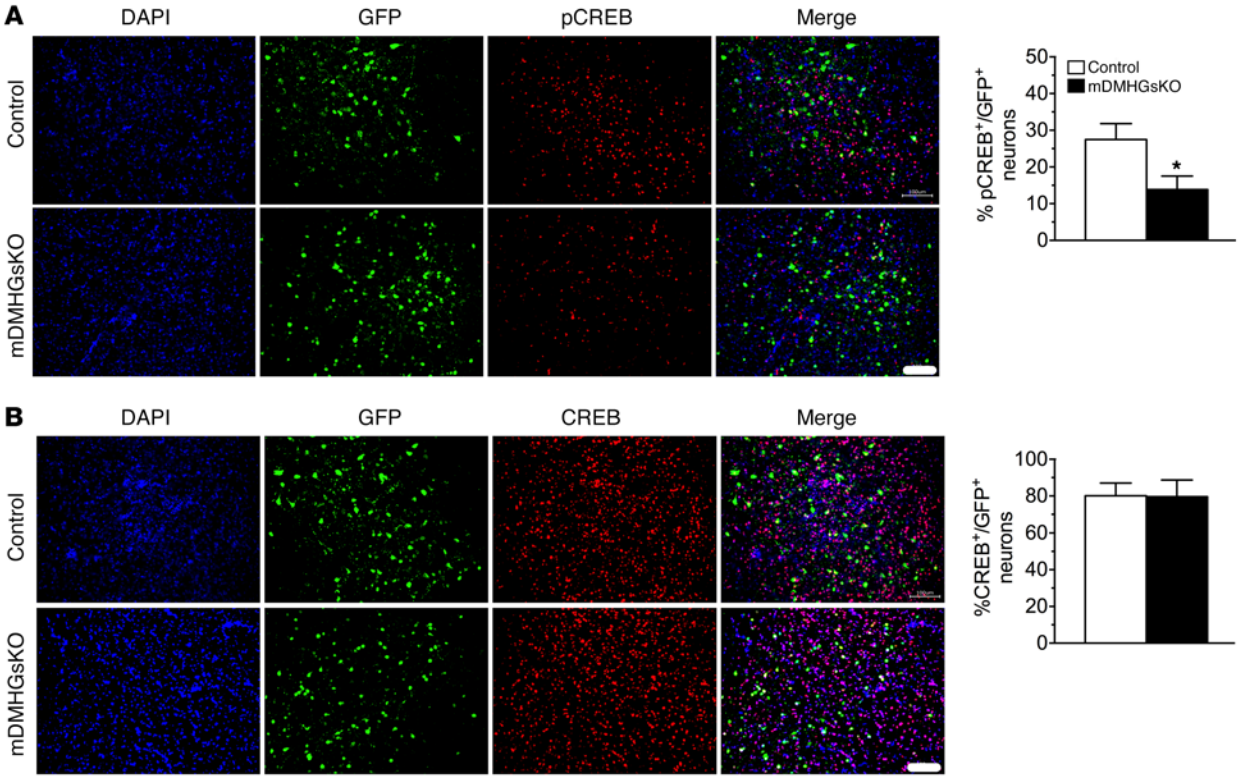

Figure 6. Reduced MTII-stimulated CREB phosphorylation in the DMH of mDMHGsKO mice. (**A**) Representative images of the DMH (dorsal and compact area) showing DAPI staining, GFP staining, pCREB staining, and merged images from control and mDMHGsKO mice after i.p. MTII administration. Right panel shows quantification of percentage of GFP$^+$ neurons that are also pCREB$^+$ (n = 9–10). Baseline pCREB staining in control mice after saline injection was very low (7% ± 2% pCREB$^+$/GFP$^+$ neurons; not shown). (**B**) Representative images of the DMH (dorsal and compact area) showing DAPI staining, GFP staining, total CREB protein staining, and merged images from control and mDMHGsKO mice after MTII administration. Right panel shows quantification of the percentage of GFP$^+$ neurons that are also CREB$^+$ (n = 4–5). Scale bars: 100 μm. Data are shown as mean ± SEM. *P < 0.05 vs. controls by Student's t test.

neurons in cold-induced thermogenesis, as mDMHGsKO mice do not have a complete (homozygous) loss of $G_s\alpha$ in the DMH. While MC4Rs are also necessary for cold-induced thermogenesis, loss of MC4R in the DMH is not sufficient to impair cold induction of thermogenesis. Rather, this effect has been shown to primarily involve MC4Rs in sympathetic preganglionic neurons (38).

The DMH-medullary raphe circuit is also believed to evoke cardiac SNS activity. We observed that mDMHGsKO mice had reduced heart rate, but normal blood pressure. In contrast, mice with whole-brain and PVN–specific *Gnas* knockout have both decreased heart rate and blood pressure (9), consistent with $G_s\alpha$ pathways in the PVN being the primary mediator of MC4R effects on blood pressure (27, 39). The present results suggest that $G_s\alpha$ signaling in different hypothalamic nuclei plays different roles in regulating cardiovascular function.

Impaired CNS MC4R (21, 40, 41) and $G_s\alpha$ signaling (8) have both been shown to have a primary effect on glucose metabolism and insulin action independent of their effects on adiposity. We previously showed that $G_s\alpha$ deficiency in the PVN does not have a primary effect on glucose metabolism (9). While mDMHGsKO and DMH-MC4RKO mice develop glucose intolerance and insulin resistance after becoming obese, no abnormalities in glucose metabolism or insulin sensitivity were observed in either group of mice at 2 weeks after viral injection at a time point before the development of obesity. These results suggest that loss of MC4R-$G_s\alpha$ signaling in the DMH is not sufficient to produce the primary abnormalities in glucose metabolism seen with more global mutation of $G_s\alpha$ or MC4R. A recent study showed that effects of central melanocortins on peripheral glucose metabolism and insulin action are the result of MC4R action in cholinergic autonomic preganglionic neurons (38).

In conclusion, our results reveal the CNS site where $G_s\alpha$ imprinting leads to the parent-of-origin–specific metabolic phenotype observed in mice and provide a plausible mechanism for the development of obesity in AHO patients. While the onset of obesity is early (first year of life) in AHO patients and later in *Gnas* knockout models (6 to 7 weeks), it should be noted that MC4R mutations show a very similar discrepancy between the time of onset of obesity in humans (first year of life) versus mice (5 weeks) (22, 23). In addition, we directly show that MC4R-$G_s\alpha$ signaling in the DMH is important for stimulation of energy expenditure and BAT activation, although cold-induced BAT activation is not dependent on MC4R-$G_s\alpha$ signaling in the DMH. While we focused on the role of $G_s\alpha$ in melanocortin signaling, it is likely that the effect of $G_s\alpha$ mutations on signaling from other receptors also contributes to the observed phenotypes. It is also possible that $G_s\alpha$ signaling is normally involved in other important regulatory pathways that would only be observable in a complete (homozygous) knockout.

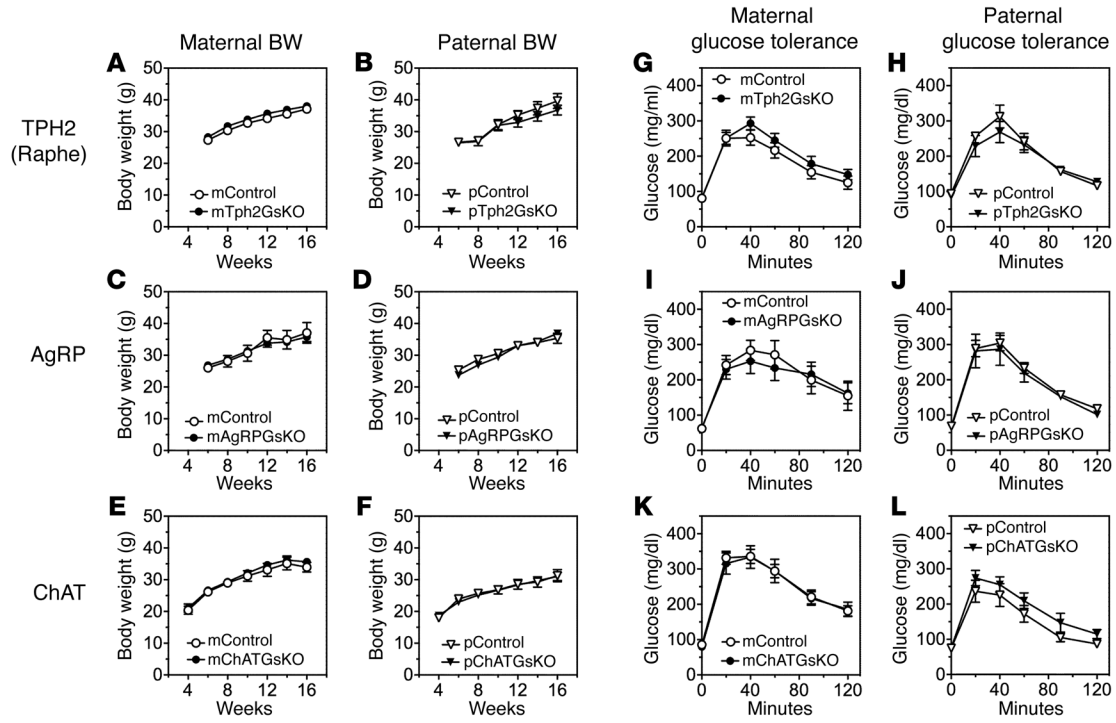

Figure 7. Absence of a metabolic phenotype in male mice with maternal or paternal $G_s\alpha$ deficiency in distinct neuronal populations. (**A**, **C**, and **E**) Body weight curves in mice with (**A**) maternal $G_s\alpha$ deletion in serotonergic (TPH2) neurons (n = 9–14/group), (**C**) AgRP neurons (n = 6–7/group), or (**E**) ChAT neurons (n = 7–9/group) and their control littermates. (**B**, **D**, and **F**) Body weight curves in mice with paternal $G_s\alpha$ deletion in (**B**) TPH2 neurons (n = 4/group), (**D**) AgRP neurons (n = 6-10/group), or (**F**) ChAT neurons (n = 6–8/group) and their control littermates. (**G**, **I**, and **K**) Glucose tolerance tests in mice with maternal $G_s\alpha$ deletion in (**G**) TPH2 neurons (n = 9–13/group), (**I**) Agrp neurons (n = 4–5/group), or (**K**) ChAT neurons (n = 7–8/group) and their control littermates. (**H**, **J**, and **L**) Glucose tolerance tests in mice with paternal $G_s\alpha$ deletion in (**H**) TPH2 neurons (n = 4/group), (**J**) AgRP neurons (n = 3–7/group), or (**L**) ChAT neurons (n = 7–11/group) and their control littermates. Data are shown as mean ± SEM.

Methods

Mice. Mice with loxP sites surrounding *Gnas* exon 1 ($E1^{fl/fl}$) were generated as previously described (42). Floxed *Mc4r* (*Mc4r*$^{fl/fl}$) mice were gift from B. Lowell (Beth Israel Deaconess Medical Center, Boston, Massachusetts, USA) (43). To generate heterozygotes with disruption of the maternal $G_s\alpha$ allele in AgRP-expressing neurons (mAgRPGsKO), female $E1^{fl/fl}$ mice were mated with male *Agrp-Cre* mice (The Jackson Laboratory). To generate heterozygotes with disruption of the maternal $G_s\alpha$ allele in ChAT-expressing neurons (mChATGsKO), female $E1^{fl/fl}$ mice were mated with male *Chat-Cre* mice (The Jackson Laboratory). To generate heterozygotes with disruption of the maternal $G_s\alpha$ allele in serotoninergic neurons (mTph2GsKO), female $E1^{fl/fl}$ mice were mated with males containing a tamoxifen-inducible *Cre* gene driven by the *Tph2* promoter (*Tph2-CreER*^{T2}, a gift of D. Bartsch, Heidelberg University, Mannheim, Germany), and tamoxifen (1 mg) was i.p. injected into 6-week-old mice twice daily for 5 consecutive days (44). Paternal heterozygotes (pAgRPGsKO, pChATGsKO, pTph2GsKO) were generated by respective reciprocal crosses. Littermates lacking the *Cre* genes were used as controls. Mice with heterozygous germline $G_s\alpha$ deletion on either the maternal ($E1^{m-}$) or paternal ($E1^{p-}$) allele were generated as previously described (4).

Genotyping was performed by PCR as previously described (42). Primers to determine the presence of the E1 flox site were 5′-TTCGGTCTCGTCCCCTTAGTTG-3′ (forward) and 5′-AACAAATCGCACACCCCAGTGAGG-3′(reverse); primers for the *Cre* gene were 5′-CCTGTTTTGCACGTTCACCG-3′ (forward) and 5′-ATGCTTCTGTCCGTTTGCCG-3′ (reverse); and primers for α-tubulin (internal control for amplification) were 5′-GTGGGTTCCAGGTCTACGAA-3′ (forward) and 5′AGACCATTGGGGGAGGAGAT-3′ (reverse). Mice were maintained on a 12-hour light/12-hour dark cycle (6 am/6 pm) and chow diet (NIH-07, 5% fat by weight). Unless noted, animals were studied at 2 to 2.5 months after stereotaxic viral injection or at age 3 to 4 months for other mouse lines.

Stereotaxic viral injections. mDMHGsKO and pDMHGsKO mice were generated by stereotaxic injection of AAV-Cre-GFP into the DMH of maternal ($E1^{fl/+}$) and paternal ($E1^{+/fl}$) $G_s\alpha$-floxed mice, while DMH-MC4RKO mice were generated by injection of AAV-Cre-GFP into the DMH of homozygous *Mc4r*$^{fl/fl}$ mice. In all cases, 6- to 7-week-old male mice were bilaterally injected with 1.1×10^9 genomic copies/200 nl of AAV-Cre-GFP (AV-2-PV-2004, Penn Vector Core, Philadelphia, Pennsylvania, USA), while control mice were bilaterally injected with 1.4×10^9 genomic copies/200 nl of AAV-GFP (AV-2-PV0101, Penn Vector Core) at bregma: anterio-posterior (–1.88 mm), mediolateral (±0.3 mm), and dorsoventral (–5.125 mm) using a stereotaxic apparatus. Surgery was performed under isoflurane anesthesia (5% induction, 1.5%–2.5% maintenance via inhalation). The injection position was confirmed by GFP expression in the DMH using fluorescence microscopy (Supplemental Figure 1), and only data from mice with bilateral DMH injections were used.

Food intake, body composition, and energy expenditure. Food intake was measured for single-caged mice every other day for 2 weeks. Body composition was measured in nonanesthetized mice using the Echo 3 in1 NMR analyzer (Echo Medical Systems). Energy expenditure

was determined over a 24-hour period by indirect calorimetry using a 12-chamber CLAMS system (Columbus Instruments) after 48 hours of acclimation, and resting energy expenditure was determined as the means of points measured when mice were not ambulating. Total and ambulating activities were determined by infrared beam interruption.

Responses to MTII. For food-intake response, single-caged mice received MC3R/MC4R agonist MTII (200 μg i.p., Sigma-Aldrich) or vehicle (saline, 100 μl i.p.) 30 minutes before lights out, and food intake was measured for 3.5 hours in the dark. For energy expenditure response, mice were placed in indirect calorimetry chambers for 24 hours at 30°C and received MTII (10 μg/g i.p.) or saline on the following day at 1,000 hours. Total O_2 consumption was measured for 3 hours after injection, excluding the first 1.5 hours after injection.

CREB phosphorylation in DMH. Brains were collected at 60 minutes after injection with MTII (10 μg/g i.p.). Brain sections were pretreated with heat-mediated antigen retrieval by incubation in sodium citrate buffer (10 mM sodium citrate, 0.05% Tween 20, pH 6.0) at 95°C for 30 minutes. Sections were then blocked in 5% horse serum (Vector Laboratories) plus 0.3% Triton X-100 at room temperature for 1.5 hours and then incubated with anti–phospho-CREB (Ser133) antibody (Cell Signaling Technology, catalog 9191) or anti-CREB antibody (Cell Signaling Technology, catalog 4820) and anti-GFP antibody (Life Technologies, catalog A10262) in 2.5% horse serum plus 0.3% Triton X-100 overnight in 4°C, followed by incubation with Alexa Fluor–conjugated secondary antibodies (Alexa Fluor 555 for pCREB and CREB [Life Technologies, catalog A21429]; Alexa Fluor 488 for GFP [Life Technologies, catalog A11039]). Imaging and quantification were performed using BZ-II Analyzer software, version 2.1 (Keyence).

Glucose and insulin tolerance tests. For glucose and insulin tolerance tests, overnight-fasted mice were given i.p. glucose (2 mg/g) or insulin (Humulin, 0.75 mIU/g). Tail blood was collected before (time 0) and at indicated times after injection for measurement of glucose using Glucometer Contour (Bayer).

Blood pressure, heart rate, and body temperature. Blood pressure and heart rate were measured with a BP-2000 Specimen platform (Visitech). Core body temperature was measured with a TH-5 rectal probe (Thermalet) inserted 1 cm deep at room temperature and hourly during 4°C exposure in mice caged individually without bedding. Food and water were provided ad libitum.

In situ hybridization. To measure $G_s\alpha$ mRNA levels in the DMH, in situ hybridization was performed on brain slices from WT, $E1^{m-}$, and $E1^{p-}$ mice using a 118-bp RNA probe for *Gnas* exon 1 (coding nucleotides 5–122). To measure *Mc4r* mRNA levels in the DMH, in situ hybridization was performed on brain slices from control and DMH-MC4RKO mice using a 520-bp *Mc4r* RNA probe (cDNA bp 1180–1700; GenBank NM_016977). Frozen brain sections were fixed and incubated in 0.25% acetic anhydride and 0.1 M triethanolamine hydrochloride dissolved in 0.9% NaCl for 10 minutes and then washed and dehydrated. ^{35}S-labeled probe (10^7 cpm/ml) was added to hybridization buffer containing 50% formamide, 0.2 M NaCl, 50 mM Tris HCl, pH 8, 2.5 mM EDTA, 250 μg/ml transfer RNA (tRNA), 10% dextran sulfate, and 50 mM dithiothreitol. The sections were incubated at 55°C overnight and washed in 4× SSC, dehydrated, and immersed in buffer (0.3 mM NaCl, 50% formamide, 20 mM Tris-HCl, 1 mM EDTA) at 60°C for 15 minutes. The sections were exposed in NTB2 emulsion for 3 days after treatment with ribonuclease A (20 μg/ml). The same sections were then counterstained with H&E. RNA signals were quantified using Image-Pro Plus software (Media Cybernetics).

Biochemical assays. Serum insulin was measured by RIA (Millipore) or ELISA (Crystal Chem) and leptin by ELISA (R&D Systems). Serum-free fatty acids were measured using reagents from Roche, and triglycerides and cholesterol levels were measured using reagents from Thermo Scientific. Serum T3 and T4 levels were measured using reagents from Calbiotech. Serum corticosterone levels were measured by RIA (MP Biomedical). Serum glucose levels were measured with the Glucometer Contour (Bayer).

Quantitative RT-PCR. Total RNA was isolated from BAT using the RNeasy lipid tissue kit (QIAGEN) and treated with DNAse I (Invitrogen) at room temperature for 15 minutes. Reverse transcription was performed using MultiScribe RT (Applied Biosystems). BAT mRNA levels were measured by quantitative reverse transcriptase PCR (RT-PCR) (Applied Biosystems, StepOnePlus) in 20 μl reaction volumes including BAT cDNA (20 ng of initial RNA sample), 50 nM primers, and 10 μl of 2× Power SYBR Green Master Mix (Applied Biosystems). Results were normalized to simultaneously determined β-actin mRNA levels in each sample using comparative method software provided by StepOnePlus.

For additional information, see Supplemental Methods.

Statistics. Data are expressed as mean ± SEM and were analyzed by 2-tailed unpaired Student's *t* test with differences considered significant at $P < 0.05$.

Study approval. All animal studies were approved by the National Institute of Diabetes and Digestive and Kidney Diseases Animal Care and Use Committee.

Author contributions

MC, YBS, OG, and LSW designed the experiments. MC, YBS, BP, BN, HS, TH, EAW, ZC, YQL, and OG performed the experiments and analyzed data. MC and LSW wrote the manuscript, and all authors edited it.

Acknowledgments

We would like to thank the National Institute of Diabetes and Digestive and Kidney Diseases Mouse Metabolism Core Laboratory for technical assistance and B. Lowell and D. Bartsch for providing mouse lines. This work was supported by the Intramural Research Program of the National Institute of Diabetes and Digestive and Kidney Diseases.

Address correspondence to: Lee S. Weinstein, Metabolic Diseases Branch, NIDDK/NIH, Building 10, Room 8C101, Bethesda, Maryland 20892, USA. Phone: 301.402.2923; E-mail: leew@mail.nih.gov.

BP and TH's present address is: University of Virginia School of Medicine, Virginia, USA.

1. Long DN, McGuire S, Levine MA, Weinstein LS, Germain-Lee EL. Body mass index differences in pseudohypoparathyroidism type 1a versus pseudopseudohypoparathyroidism may implicate paternal imprinting of Galpha(s) in the development of human obesity. *J Clin Endocrinol Metab*. 2007;92(3):1073–1079.
2. Roizen JD, et al. Resting energy expenditure is decreased in pseudohypoparathyroidism type 1A. *J Clin Endocrinol Metab*. 2016;101(3):880–888.
3. Muniyappa R, et al. Reduced insulin sensitivity in adults with pseudohypoparathyroidism type 1a.

J Clin Endocrinol Metab. 2013;98(11):E1796–E1801.
4. Chen M, et al. Alternative Gnas gene products have opposite effects on glucose and lipid metabolism. *Proc Natl Acad Sci USA*. 2005;102(20):7386–7391.
5. Xie T, Chen M, Gavrilova O, Lai EW, Liu J, Weinstein LS. Severe obesity and insulin resistance due to deletion of the maternal Gsalpha allele is reversed by paternal deletion of the Gsalpha imprint control region. *Endocrinology*. 2008;149(5):2443–2450.
6. Germain-Lee EL, et al. A mouse model of albright hereditary osteodystrophy generated by targeted disruption of exon 1 of the Gnas gene. *Endocrinology*. 2005;146(11):4697–4709.
7. Weinstein LS, Xie T, Zhang QH, Chen M. Studies of the regulation and function of the Gs alpha gene Gnas using gene targeting technology. *Pharmacol Ther*. 2007;115(2):271–291.
8. Chen M, et al. Central nervous system imprinting of the G protein G(s)alpha and its role in metabolic regulation. *Cell Metab*. 2009;9(6):548–555.
9. Chen M, Berger A, Kablan A, Zhang J, Gavrilova O, Weinstein LS. Gsα deficiency in the paraventricular nucleus of the hypothalamus partially contributes to obesity associated with Gsα mutations. *Endocrinology*. 2012;153(9):4256–4265.
10. Berger A, et al. Gsα Deficiency in the ventromedial hypothalamus enhances leptin sensitivity and improves glucose homeostasis in mice on a high-fat diet. *Endocrinology*. 2016;157(2):600–610.
11. Butler AA, Cone RD. The melanocortin receptors: lessons from knockout models. *Neuropeptides*. 2002;36(2–3):77–84.
12. Balthasar N, et al. Divergence of melanocortin pathways in the control of food intake and energy expenditure. *Cell*. 2005;123(3):493–505.
13. Dimicco JA, Zaretsky DV. The dorsomedial hypothalamus: a new player in thermoregulation. *Am J Physiol Regul Integr Comp Physiol*. 2007;292(1):R47–R63.
14. Morrison SF, Madden CJ, Tupone D. Central neural regulation of brown adipose tissue thermogenesis and energy expenditure. *Cell Metab*. 2014;19(5):741–756.
15. Samuels BC, Zaretsky DV, DiMicco JA. Tachycardia evoked by disinhibition of the dorsomedial hypothalamus in rats is mediated through medullary raphe. *J Physiol (Lond)*. 2002; 538(Pt 3):941–946.
16. Zaretsky DV, Zaretskaia MV, DiMicco JA. Stimulation and blockade of GABA(A) receptors in the raphe pallidus: effects on body temperature, heart rate, and blood pressure in conscious rats. *Am J Physiol Regul Integr Comp Physiol*. 2003;285(1):R110–R116.
17. Cao WH, Morrison SF. Disinhibition of rostral raphe pallidus neurons increases cardiac sympathetic nerve activity and heart rate. *Brain Res*. 2003;980(1):1–10.
18. Kataoka N, Hioki H, Kaneko T, Nakamura K. Psychological stress activates a dorsomedial hypothalamus-medullary raphe circuit driving brown adipose tissue thermogenesis and hyperthermia. *Cell Metab*. 2014;20(2):346–358.
19. Kishi T, Aschkenasi CJ, Lee CE, Mountjoy KG, Saper CB, Elmquist JK. Expression of melanocortin 4 receptor mRNA in the central nervous system of the rat. *J Comp Neurol*. 2003;457(3):213–235.
20. Mountjoy KG, Mortrud MT, Low MJ, Simerly RB, Cone RD. Localization of the melanocortin-4 receptor (MC4-R) in neuroendocrine and autonomic control circuits in the brain. *Mol Endocrinol*. 1994;8(10):1298–1308.
21. Fan W, Dinulescu DM, Butler AA, Zhou J, Marks DL, Cone RD. The central melanocortin system can directly regulate serum insulin levels. *Endocrinology*. 2000;141(9):3072–3079.
22. Farooqi IS, Keogh JM, Yeo GS, Lank EJ, Cheetham T, O'Rahilly S. Clinical spectrum of obesity and mutations in the melanocortin 4 receptor gene. *N Engl J Med*. 2003;348(12):1085–1095.
23. Huszar D, et al. Targeted disruption of the melanocortin-4 receptor results in obesity in mice. *Cell*. 1997;88(1):131–141.
24. Kublaoui BM, Holder JL, Gemelli T, Zinn AR. Sim1 haploinsufficiency impairs melanocortin-mediated anorexia and activation of paraventricular nucleus neurons. *Mol Endocrinol*. 2006;20(10):2483–2492.
25. Kublaoui BM, Holder JL, Tolson KP, Gemelli T, Zinn AR. SIM1 overexpression partially rescues agouti yellow and diet-induced obesity by normalizing food intake. *Endocrinology*. 2006;147(10):4542–4549.
26. Holder JL, Butte NF, Zinn AR. Profound obesity associated with a balanced translocation that disrupts the SIM1 gene. *Hum Mol Genet*. 2000;9(1):101–108.
27. Li YQ, et al. G(q/11)α and G(s)α mediate distinct physiological responses to central melanocortins. *J Clin Invest*. 2016;126(1):40–49.
28. Fan W, Morrison SF, Cao WH, Yu P. Thermogenesis activated by central melanocortin signaling is dependent on neurons in the rostral raphe pallidus (rRPa) area. *Brain Res*. 2007;1179:61–69.
29. Voss-Andreae A, et al. Role of the central melanocortin circuitry in adaptive thermogenesis of brown adipose tissue. *Endocrinology*. 2007;148(4):1550–1560.
30. Yasuda T, Masaki T, Kakuma T, Yoshimatsu H. Hypothalamic melanocortin system regulates sympathetic nerve activity in brown adipose tissue. *Exp Biol Med (Maywood)*. 2004;229(3):235–239.
31. Hosoya Y, Ito R, Kohno K. The topographical organization of neurons in the dorsal hypothalamic area that project to the spinal cord or to the nucleus raphé pallidus in the rat. *Exp Brain Res*. 1987;66(3):500–506.
32. Nakamura K, et al. Identification of sympathetic premotor neurons in medullary raphe regions mediating fever and other thermoregulatory functions. *J Neurosci*. 2004;24(23):5370–5380.
33. Cao WH, Fan W, Morrison SF. Medullary pathways mediating specific sympathetic responses to activation of dorsomedial hypothalamus. *Neuroscience*. 2004;126(1):229–240.
34. Zhang Y, et al. Leptin-receptor-expressing neurons in the dorsomedial hypothalamus and median preoptic area regulate sympathetic brown adipose tissue circuits. *J Neurosci*. 2011;31(5):1873–1884.
35. Enriori PJ, Sinnayah P, Simonds SE, Garcia Rudaz C, Cowley MA. Leptin action in the dorsomedial hypothalamus increases sympathetic tone to brown adipose tissue in spite of systemic leptin resistance. *J Neurosci*. 2011;31(34):12189–12197.
36. Nakamura Y, Nakamura K, Matsumura K, Kobayashi S, Kaneko T, Morrison SF. Direct pyrogenic input from prostaglandin EP3 receptor-expressing preoptic neurons to the dorsomedial hypothalamus. *Eur J Neurosci*. 2005;22(12):3137–3146.
37. Tupone D, Madden CJ, Morrison SF. Autonomic regulation of brown adipose tissue thermogenesis in health and disease: potential clinical applications for altering BAT thermogenesis. *Front Neurosci*. 2014;8:14.
38. Berglund ED, et al. Melanocortin 4 receptors in autonomic neurons regulate thermogenesis and glycemia. *Nat Neurosci*. 2014;17(7):911–913.
39. Li P, Cui BP, Zhang LL, Sun HJ, Liu TY, Zhu GQ. Melanocortin 3/4 receptors in paraventricular nucleus modulate sympathetic outflow and blood pressure. *Exp Physiol*. 2013;98(2):435–443.
40. Obici S, Feng Z, Tan J, Liu L, Karkanias G, Rossetti L. Central melanocortin receptors regulate insulin action. *J Clin Invest*. 2001;108(7):1079–1085.
41. Nogueiras R, et al. The central melanocortin system directly controls peripheral lipid metabolism. *J Clin Invest*. 2007;117(11):3475–3488.
42. Chen M, et al. Increased glucose tolerance and reduced adiposity in the absence of fasting hypoglycemia in mice with liver-specific Gs alpha deficiency. *J Clin Invest*. 2005;115(11):3217–3227.
43. Shah BP, et al. MC4R-expressing glutamatergic neurons in the paraventricular hypothalamus regulate feeding and are synaptically connected to the parabrachial nucleus. *Proc Natl Acad Sci U S A*. 2014;111(36):13193–13198.
44. Weber T, Böhm G, Hermann E, Schütz G, Schönig K, Bartsch D. Inducible gene manipulations in serotonergic neurons. *Front Mol Neurosci*. 2009;2:24.